Excitation of highly oblique lower band and upper band chorus by a loss-cone feature and temperature anisotropy distribution

Qinghua Zhou,[1,2,3] Chang Yang,[1] Yihua He,[1] Si Liu,[1] Zhonglei Gao,[1] Fuliang Xiao[1,2,3]

F. Xiao, School of Physics and Electronic Sciences, Changsha University of Science and Technology, Changsha, 410114, China. (flxiao@126.com)

[1]School of Physics and Electronic Sciences, Changsha University of Science and Technology, Changsha, China.

[2]Hunan Provincial Key Laboratory of Flexible Electronic Materials Genome Engineering, Changsha University of Science and Technology, Changsha, China.

[3]Hunan Province Higher Education Key Laboratory of Modeling and Monitoring on the Near-Earth Electromagnetic

This article has been accepted for publication and undergone full peer review but has not been through the copyediting, typesetting, pagination and proofreading process, which may lead to differences between this version and the Version of Record. Please cite this article as doi: 10.1029/2018GL081379

Recent studies have indicated that highly oblique lower band chorus could be excited by temperature anisotropy with a low-energy electron plateau. Here we present another excitation mechanism of highly oblique lower and upper band chorus by using the simultaneous observations and numerical modeling. During 23:00-24:00 UT on 3 July 2016, Van Allen probe A observed chorus with the wave normal angle close to the resonance cone both in the lower and upper bands around $L = 5.0$ and MLT = 3. Enhanced flux and pitch angle anisotropy of energetic electrons were observed in the same spatial region. Calculations of chorus growth rates show that highly oblique chorus waves can be excited by the energetic electrons with a loss-cone feature and distinct temperature anisotropy, particularly more efficient in the presence of a low-energy plateau. The temperature anisotropy for the oblique upper band is higher than that for the lower band.

Environments, Changsha University of Science and Technology, Changsha, China.

1. Introduction

Whistler-mode chorus is right hand polarized electromagnetic waves propagating outside the plasmapause between 22 and 13 magnetic local time (MLT). They are typically observed in a lower band 0.1-0.5 f_{ce} (f_{ce} is the electron gyrofrequency) and upper band 0.5-0.8 f_{ce}, with a minimum wave power at $0.5f_{ce}$ [*Tsurutani and Smith*, 1974]. Based on the data from the Double Star TC-1 spacecraft, *Santolík et al.* [2005] have reported the radial variation of chorus: the upper band chorus disappears for $L > 8$, while the lower band chorus is observed up to L = 11-12. It is generally accepted that the source region of chorus waves is located outside the plasmapause near the geomagnetic equator [*Parrot et al.*, 2003a]. They encounter magnetospheric reflection at the high magnetic latitude (λ) in propagation upward [*Parrot et al.*, 2003b; *Santolík et al.*, 2006]. Previous calculation results have shown that oblique chorus with initial wave vector **k** pointing toward the Earth can propagate into the plasmasphere and evolve into plasmaspheric hiss [*Bortnik et al.*, 2008, 2011; *Chen et al.*, 2009; *Zhou et al.*, 2016].

Earlier studies have suggested that the wave normal angle of lower band chorus is generally confined within 20°, while upper band chorus occurs with a broad range of wave normal angles. Recently, *Li et al.* [2013] and *Agapitov et al.* [2013] have shown the presence of a significant population of oblique chorus with a large wave normal angle close to the resonance cone angle $\theta_R = \arccos(f/f_{ce})$ using THEMIS and Cluster data, and *Li et al.* [2016a] have further confirmed it using more precise Van Allen Probes data. Most of these highly oblique chorus waves occur during quiet or modest geomagnetic activity at relatively lower L shells ($L \approx 4-5.5$). Highly oblique chorus waves could be generated

by Landau resonance with a low-energy electron beam or by cyclotron resonance with temperature anisotropic keV electrons in the presence of a low-energy electron plateau [*Mourenas et al.*, 2015; *Artemyev et al.*, 2016]. These excitation mechanisms have been confirmed by the simultaneous observations of Van Allen Probes [*Li et al.*, 2016b]. Based on the nonlinear theory, *Fu et al.* [2017] proposed the three-wave resonance mechanism for the excitation of highly oblique chorus waves, and *Teng et al.* [2018] presented the relevant observational evidence. Highly oblique chorus can provide efficient energy diffusion for the rapid acceleration of electrons [*Artemyev et al.*, 2016]. The electron pitch angle scattering rates driven by highly oblique chorus could be stronger than those by quasi-parallel waves with the same wave amplitudes [*Li et al.*, 2014]. Therefore, the role of highly oblique chorus waves in radiation belt dynamics should not be neglected. Previous works have not explained the excitation mechanism of highly oblique upper band chorus. Here we present another mechanism that highly oblique lower and upper band chorus waves can be excited by the energetic electrons with a loss-cone distribution and distinct temperature anisotropy.

2. Observation

During 23:00-24:00 UT on 3 July 2016, a highly oblique chorus waves event was observed by Van Allen Probe A. The spectral data of wave electric field at frequencies between 10 and 500 kHz are provided by the High Frequency Receiver (HFR) and the complete spectral matrices of waves for 10 Hz to 12 kHz are provided by the waveform receiver (WFR) of Electric and Magnetic Field Instrument Suite and Integrated Science (EMFISIS), respectively [*Kletzing et al.*, 2013]. The differential flux j of electrons with energies between

$\sim$10 eV and $\sim$50 keV is measured at different pitch angles by the Helium Oxygen Proton Electron (HOPE) mass spectrometer [*Spence et al.*, 2013; *Funsten et al.*, 2013].

Figure 1a shows the geomagnetic disturbance index SYM_H between -15 and 15 nT on 3 July 2016, corresponding to the relatively quiet geomagnetic activity. Figures 1b-1d show the wave power spectra measured by the EMFISIS instrumentation suite of Probe A during 23:00-24:00 UT (corresponding to the shaded area in Figure 1a). The upper hybrid resonance frequency dropped to $\sim$20 kHz, indicating that Probe A was beyond the plasmapause. Enhanced electromagnetic waves were observed in the region of MLT = 2.7-3.7 and λ = 8.7°-11.1° south, with a lower band $\sim$ 0.2-0.5 f_{ce} during 23:08-24:00 UT, and an upper band $\sim$0.5-0.7 f_{ce} during 23:08-23:25 UT. Figures 1e-1f show the wave normal angle (θ) and ellipticity calculated with the singular value decomposition technique [*Santolík et al.*, 2003]. The wave normal angle $\theta \approx 50°$ at $0.7f_{ce}$, and increased to $\sim$80° at $0.2f_{ce}$, both close to the resonance cone $\theta_R \approx 46°$ at $0.7f_{ce}$ and 79° at $0.2f_{ce}$. The waves were right-hand polarized (the ellipticity $\approx$ 1). Therefore, the enhanced electromagnetic waves were identified as highly oblique chorus waves.

Figure 2a shows the electron density derived from the upper hybrid frequency (the white line in Figure 1b) [*Kurth et al.*, 2015]. The electron density decreased rapidly from $\sim$50 cm^{-3} to $\sim$5 cm^{-3} during the period of 23:00-23:10 UT, and gradually to $\sim$2 cm^{-3} around 24:00 UT. Figures 2b-2c demonstrate that electron pitch angle anisotropy from the HOPE instrument was pronounced for the energy range 2.5-12 keV. At the same time, the fluxes of the energetic (2.5-12 keV) electrons increased by 1-2 orders of magnitude (Figures 2b-2c).

3. Numerical Calculations

We calculate local growth rates (γ) of chorus waves following the method introduced by *Chen et al.* [2010], and compare them with the observation. The electron distribution for the growth rate is derived based on the electron PSD from HOPE and assumed to be a sum of six components.Each component assumes the form:

$$f_i(v_\parallel, v_\perp) = \frac{N_i}{\pi^{3/2}\theta_{\perp i}^2\theta_{\parallel i}} \exp\Big(-\frac{(v_\parallel - v_{di}))^2}{\theta_{\parallel i}^2}\Big)\Big[\Delta_i \exp\Big(-\frac{v_\perp^2}{\theta_{\perp i}^2}\Big) + \frac{(1-\Delta_i)}{(1-\beta_i)}\Big(\exp\Big(-\frac{v_\perp^2}{\theta_{\perp i}^2}\Big) - \exp\Big(-\frac{v_\perp^2}{\beta_i\theta_{\perp i}^2}\Big)\Big)\Big], \quad (1)$$

where N_i is the number density of electron component i, v_{di} is the beam velocity in the direction parallel to the background magnetic field. $\theta_{\parallel i}$ and $\theta_{\perp i}$ are the thermal velocities parallel and perpendicular to the ambient magnetic field, respectively. Δ_i and β_i are parameters in the range 0-1.0 to describe the loss-cone feature. The distribution function incorporates the plateau in the parallel PSD, the loss-cone feature, and the temperature anisotropy. When $v_d = 0$, it reduces to the subtracted bi-Maxwellian distribution [*Ashour-Abdalla and Kennel*, 1978]. If $v_d = 0$, $\Delta = 1$ and $\beta \to 0$, it reduces to the bi-Maxwellian distribution. We define the total anisotropy parameter A_{total} of each electron component

$$A_{total} = A_T + A_L \quad (2)$$

$$A_T = \frac{\theta_\perp^2}{\theta_\parallel^2} \quad (3)$$

$$A_L = \beta(1-\Delta)\frac{\theta_\perp^2}{\theta_\parallel^2}, \quad (4)$$

where A_T is defined as the temperature anisotropy, and A_L is defined as the loss-cone anisotropy.

Two time periods A and B (Figure 1) are chosen to investigate the excitation mechanisms of highly oblique upper band and lower band chorus. Continuous lower band chorus occurred at both times A and B, while upper band chorus occurred only at the time A. The discrete asterisks in Figure 3 represent the PSD of electrons measured by the HOPE instrument at times A and B, respectively. The temperature anisotropy becomes distinct for the velocity above $\sim 6 \times 10^6$ m/s at times A and B. The loss-cone feature appears for the velocity in the range $3.5 - 4.7 \times 10^7$ m/s (or $1.8 - 2.7 \times 10^7$ m/s) at the time A (or B). The small plateau feature in the parallel electron velocity distribution occurred at the velocity in the range $2.1 - 2.6 \times 10^7$ m/s (or $1.0 - 1.6 \times 10^7$ m/s) at the time A (or B). A subtracted bi-Maxwellian component with the transverse thermal velocity close to 4.0×10^7 m/s (or 2.2×10^7 m/s) is adopted to reproduce the loss-cone feature in PSD at the time A (or B). A beam component with the beam velocity close to 2.3×10^7 m/s (or 1.3×10^7 m/s) is adopted to fit the plateau in the parallel PSD at the time A (or B). The other four components are bi-Maxwellian distributions. The solid lines in Figure 3 show the fits to the observed electron PSD. The fitted parameters are obtained by performing the nonlinear least squares fitting [*Marquardt*, 1963] and listed in Table 1.

The equatorial ambient magnetic field B_0 which is used to calculate electron equatorial gyrofrequency f_{ce} (or equatorial angular gyrofrequency Ω_{ce}) is obtained from the Ephemeris data of Van Allen Probe A based on the T89D magnetic model. The density of the background electron (N_c) is assumed to be the difference between the observed electron density (Figure 2a) and the sum of N_i in Table 1. For each wave frequency, different wave normal angles correspond to different growth rates. In Figure 4, we plot

the maximum growth rate at each frequency, reached for a specific wave normal angle. For the time A, distinct chorus instability occurs in both lower and upper bands with a gap around the frequency $f = 0.55f_{ce}$. The growth rate has peaks $\approx 3.9\times10^{-4}$ and 1.6×10^{-4} at $0.35f_{ce}$ and $0.65f_{ce}$, respectively. For the time B, the growth rate has a peak $\approx 3.0\times10^{-4}$ at $0.39f_{ce}$ in the lower band. The calculated wave frequency and normal angle distribution are generally consistent with the observation. Because the wave parallel group velocity is roughly equal to the Landau resonant velocity $v_{\|} \approx$ 10,000 km/s at $L \approx$ 4.8-5.3, it takes ~0.6 s for chorus to travel from the magnetic equator to the observed location $\lambda \approx 10^{\circ}$ (the propagation distance ~6000 km). The obtained growth rate $\gamma \sim 4 \times 10^{-4}\Omega_{ce}$ allows the wave amplitude to increase by 20 dB in ~0.6 s. This indicates that the current mechanism is viable though the obtained growth rate is 1.5 to 3 times smaller than ones obtained in other events when considering different generation mechanisms ([*Li et al.*, 2016b; *Fu et al.*, 2017]). It should be mentioned that, as shown in Table S1 and Figure S1, we have also fit the data using multiple beam components without loss-cone component, but the calculated growth rates are zero, i.e., there is not any chorus growth. Hence, the adopted loss-cone component (though a relatively small proportion) here is essential to excitation of the highly oblique chorus wave in this case.

To understand the effect of plateau feature, temperature anisotropy and loss-cone feature on the highly oblique chorus growth rates, we calculate chorus growth rates excited by energetic electrons composed of a beam component and a subtracted bi-Maxwellian component using different parameters shown in Table 2. Calculations are performed with $N_c = 1 \times 10^6$ m^{-3} and $L = 5$. As shown in Figure 5a, the lower-band chorus growth rates

in the presence of a beam component with $v_d = 1.5 \times 10^7$ m/s (or 2.5×10^7 m/s) are about 1.5 (or 2.3) times higher than those in the absence of a beam component. For the upper band, local growth rates decrease slightly with the increase of v_d. The results confirm the previous finding that low-energy electron beams can reduce the Landau damping of oblique lower band chorus and lead to a stronger growth rate [*Mourenas et al.*, 2015; *Li et al.*, 2016b]. The results in Figure 5b demonstrate that upper band instability occurs only for temperature anisotropy of the subtracted bi-Maxwellian component $A_T = 1.8$, but is absent for $A_T = 1$ or 1.4. This explains why the highly oblique chorus waves occurred in both the lower band and the upper band at the time A ($A_T \approx 1.89$) but only in lower band at the time B ($A_T \approx 1.47$). As shown in Figures 5c-5d, the instability of highly oblique chorus waves is very sensitive to the loss-cone parameters Δ and β representing the depth and width of the loss-cone, respectively. Local growth rates are negligible when $\Delta \geq 0.4$, and increase by about 2 times when Δ decreases from 0.2 to 0.1. The upper band instability occurs only when β is very large (e.g. $\beta = 0.9$). For the lower band, when β increases from 0.2 to 0.9, the peak growth rate varies from $\sim 0.8 \times 10^{-4}$ to $\sim 2.8 \times 10^{-4}$ and moves from the frequency $0.30 f_{ce}$ to $0.40 f_{ce}$.

4. Summary

In this study, we have presented simultaneously observation of highly oblique chorus and energetic electrons by Van Allen Probe A during 23:00-24:00 UT on 3 July 2016. In order to investigate the excitation mechanism of highly oblique chorus waves, we have fitted the observed electron PSD with a sum of six components. The fitting functions

have been used to calculate chorus growth rates using different wave frequency and wave normal angle. The main results can be summarized as follows:

1. The oblique chorus waves occurred in both lower and upper bands (during 23:08-23:25 UT) and then only in the lower band (during 23:25-24:00 UT). In the meantime, energetic electrons injected from the plasmasheet display distinct temperature anisotropy and loss-cone features. At 23:18:11 UT, the growth rate has peaks $\approx 3.9\times10^{-4}$ and 1.6×10^{-4} at $0.35f_{ce}$ and $0.65f_{ce}$, respectively. At 23:54:07 UT, the growth rate has a peak $\approx 3.0\times10^{-4}$ at $0.39f_{ce}$ in the lower band. The calculated wave frequency and normal angle distribution are generally consistent with the observation. The amplitude of the chorus waves can increase by 20 dB as they travel from the equator to the observed position. This implies that the proposed mechanism is realistic though the obtained growth rates are slightly smaller than those in the previous studies using different generation mechanisms ([*Li et al.*, 2016b; *Fu et al.*, 2017]).

2. The effect of loss-cone feature, temperature anisotropy and plateau feature on the local growth rate is studied. Local growth rates increase with decreasing Δ or increasing β, indicating that the free energy coming from the loss-cone feature of electrons is critical to the excitation of highly oblique chorus. The threshold condition of the temperature anisotropy for the oblique upper band chorus is higher than that for the oblique lower band chorus. Local growth rates of oblique lower band chorus excited by electrons including the beam component are greater than those without the beam component.

The current results provide a further evidence that some lower band and upper band chorus can be excited by the energetic electrons with a loss-cone feature and distinct

temperature anisotropy in the presence of a low-energy plateau. In the future, we plan to perform a statistical study of these features in the electron distribution associated with highly oblique chorus events.

Acknowledgments. This work is supported by the National Natural Science Foundation of China grants 41674166, 41531072, 41774194, 41804171, and Scientific Research Fund of Hunan Provincial Education Department under Grant No. 16K003. All the Van Allen Probes data are publicly available at https://emfisis.physics.uiowa.edu/data/index by the EMFISIS instrument and at http://www.rbsp-ect.lanl.gov/data_pub/ by the HOPE instrument.

References

Agapitov, O., A. Artemyev, V. Krasnoselskikh, Y. V. Khotyaintsev, D. Mourenas, H. Breuillard, M. Balikhin, and G. Rolland (2013), Statistics of whistler-mode waves in the outer radiation belt: Cluster STAFF-SA measurements, *J. Geophys. Res. Space Physics*, *118*, 3407–3420, doi:10.1002/jgra.50312.

Artemyev, A., O. Agapitov, D. Mourenas, V. Krasnoselskikh, V. Shastun, and F. Mozer (2016), Oblique whistler-mode waves in the Earth's inner magnetosphere: Energy distribution, origins, and role in radiation belt dynamics, *Space Science Reviews*, *200*, 261–355, doi:10.1007/s11214-016-0252-5.

Ashour-Abdalla, M., and C. Kennel (1978), Nonconvective and convective electron cyclotron harmonic instabilities, *J. Geophys. Res.*, *83*, 1531–1543, doi:10.1029/JA083iA04p01531.

Bortnik, J., R. M. Thorne, and N. P. Meredith (2008), The unexpected origin of plasmaspheric hiss from discrete chorus emissions, *Nature*, *452*, 62–66, doi:10.1038/nature06741.

Bortnik, J., L. Chen, W. Li, R. M. Thorne, and R. B. Horne (2011), Modeling the evolution of chorus waves into plasmaspheric hiss, *J. Geophys. Res.*, *116*, A08,221, doi:10.1029/2011JA016499.

Chen, L., J. Bortnik, R. M. Thorne, R. Horne, and V. K. Jordanova (2009), Threedimensional ray tracing of VLF waves in a magnetospheric environment containing a plasmaspheric plume, *Geophys. Res. Lett.*, *36*, L22,101, doi:10.1029/2009GL040451.

Chen, L., R. M. Thorne, V. K. Jordanova, C.-P. Wang, M. Gkioulidou, L. Lyons, and R. B. Horne (2010), Global simulation of emic wave excitation during the 21 april 2001 storm from coupled rcm-ram-hotray modeling, *J. Geophys. Res.*, *115*, A07,209, doi:10.1029/2009JA015075.

Fu, X., S. P. Gary, G. D. Reeves, D. Winske, and J. R. Woodroffe (2017), Generation of highly oblique lower band chorus via nonlinear three-wave resonance, *Geophysical Research Letters*, *44*, 9532–9538, doi:10.1002/2017GL074411.

Funsten, H. O., et al. (2013), Helium, Oxygen, Proton, and Electron (HOPE) Mass Spectrometer for the Radiation Belt Storm Probes Mission, *Space Sci. Rev.*, *179*, 423–484, doi:10.1007/s11214-013-9968-7.

Kletzing, C. A., et al. (2013), The Electric and Magnetic Field Instrument Suite and Integrated Science (EMFISIS) on RBSP, *Space Sci. Rev.*, *179*, 127–181, doi:10.1007/s11214-013-9993-6.

Kurth, W. S., S. D. Pascuale, J. B. Faden, C. A. Kletzing, G. B. Hospodarsky, S. Thaller, and J. R. Wygant (2015), Electron densities inferred from plasma wave spectra obtained by the Waves instrument on Van Allen Probes, *J. Geophys. Res. Space Physics*, *120*, 904–914, doi:10.1002/2014JA020857.

Li, W., et al. (2013), Characteristics of the Poynting flux and wave normal vectors of whistler-mode waves observed on THEMIS, *J. Geophys. Res. Space Physics*, *118*, 1461–1471, doi:10.1002/jgra.50176.

Li, W., et al. (2014), Evidence of stronger pitch angle scattering loss caused by oblique whistler-mode waves as compared with quasi-parallel waves, *Geophys. Res. Lett.*, *41*, 6063–6070, doi:10.1002/2014GL061260.

Li, W., O. Santolik, J. Bortnik, R. M. Thorne, C. A. Kletzing, W. S. Kurth, and G. B. Hospodarsky (2016a), New chorus wave properties near the equator from van allen probes wave observations, *Geophys. Res. Lett.*, *43*, 4725–4735, doi:10.1002/2016GL068780.

Li, W., et al. (2016b), Unraveling the excitation mechanisms of highly oblique lower band chorus waves, *Geophys. Res. Lett.*, *43*(17), 8867–8875, doi:10.1002/2016GL070386.

Marquardt, D. W. (1963), An algorithm for least-squares estimation of nonlinear parameters, *J. Soc. Indust. Appl. Math.*, *11*, 431.

Mourenas, D., A. V. Artemyev, O. V. Agapitov, V. Krasnoselskikh, and F. S. Mozer (2015), Very oblique whistler generation by low-energy electron streams, *J. Geophys. Res. Space Physics*, *120*, 3665–3683, doi:10.1002/2015JA021135.

Parrot, M., O. Santolík, N. Cornilleau-Wehrlin, M. Maksimovic, and C. C. Harvey (2003a), Source location of chorus emissions observed by cluster, *Ann. Geophys.*, *21*, 473–480.

Parrot, M., O. Santolík, N. Cornilleau-Wehrlin, M. Maksimovic, and C. Harvey (2003b), Magnetospherically reflected chorus waves revealed by ray tracing with *cluster* data, *Ann. Geophys.*, *21*(A12), 1111–1120, doi:10.1029/2002JA009403.

Santolík, O., M. Parrot, and F. Lefeuvre (2003), Singular value decomposition methods for wave propagation analysis, *Radio Sci.*, *38(1)*, 1010, doi:10.1029/2000RS002523.

Santolík, O., E. Macúšová, K. H. Yearby, N. Cornilleau-Wehrlin, and H. S. K. Alleyne (2005), Radial variation of whistler-mode chorus: first results from the STAFF/DWP instrument on board the double star TC-I spacecraft, *Ann. Geophys.*, *23*, 2937–2942.

Santolík, O., J. Chum, M. Parrot, D. A. Gurnett, J. S. Pickett, and N. Cornilleau-Wehrlin (2006), Propagation of whistler mode chorus to low altitudes: Spacecraft observations of structured ELF hiss, *J. Geophys. Res.*, *10*, 208, doi:10.1029/2005JA011462.

Spence, H. E., et al. (2013), Science goals and overview of the Energetic Particle, Composition, and Thermal Plasma (ECT) suite on NASA's Van Allen Probes mission, *Space Sci. Rev.*, *179*, 311–336, doi:10.1007/s11214-013-0007-5.

Teng, S., J. Zhao, X. Tao, S. Wang, and G. D. Reeves (2018), Observation of oblique lower band chorus generated by nonlinear three-wave interaction, *Geophysical Research Letters*, *45*, 6343–6352, doi:10.1029/2018GL078765.

Tsurutani, B. T., and E. J. Smith (1974), Postmidnight chorus: A substorm phenomenon, *J. Geophys. Res.*, *79*, 118.

Zhou, Q., et al. (2016), Evolution of chorus emissions into plasmaspheric hiss observed by van allen probes, *J. Geophys. Res. Space Physics*, *121*, 4518–4529, doi: 10.1002/2016JA022366.

Table 1. Fitting Parameters for the Observation on 3 July 2016

Components	$N(\mathrm{m}^{-3})$	$\theta_{\parallel}$ (m/s)	$\theta_{\perp}$ (m/s)	v_d (m/s)	Δ	β
			Time A			
1	1.9×10^6	1.71×10^6	1.68×10^6	0	1	0
2	2.9×10^5	3.84×10^6	4.59×10^6	0	1	0
3	2.9×10^4	6.22×10^6	8.39×10^6	0	1	0
4	3.1×10^4	1.30×10^7	1.73×10^7	0	1	0
5	1.8×10^3	1.69×10^7	1.84×10^7	2.51×10^7	0.9	0.1
6	2.3×10^4	2.44×10^7	3.30×10^7	0	0.05	0.9
			Time B			
1	8.5×10^5	1.97×10^6	2.22×10^6	0	1	0
2	1.5×10^5	3.79×10^6	4.78×10^6	0	1	0
3	6.3×10^4	9.74×10^6	1.08×10^7	0	1	0
4	2.1×10^3	1.08×10^7	1.35×10^7	1.57×10^7	0.9	0.1
5	3.6×10^4	1.69×10^7	2.05×10^7	0	0.1	0.9
6	7.1×10^4	2.96×10^7	3.96×10^7	0	1	0

Table 2. The parameters of numerical calculations in Figure 5

Components	$N(\mathrm{m}^{-3})$	$\theta_{\parallel}$ (m/s)	$\theta_{\perp}$ (m/s)	v_d (m/s)	Δ	β
			Figure 5a			
1	2.0×10^3	1.84×10^7	1.84×10^7	varies	0.9	0.1
2	2.3×10^4	2.44×10^7	3.30×10^7	0	0.1	0.9
			Figure 5b			
1	2.0×10^3	1.84×10^7	1.84×10^7	2.5×10^7	0.9	0.1
2	2.3×10^4	2.44×10^7	varies	0	0.1	0.9
			Figure 5c			
1	2.0×10^3	1.84×10^7	1.84×10^7	2.5×10^7	0.9	0.1
2	2.3×10^4	2.44×10^7	3.30×10^7	0	varies	0.9
			Figure 5d			
1	2.0×10^3	1.84×10^7	1.84×10^7	2.5×10^7	0.9	0.1
2	2.3×10^4	2.44×10^7	3.30×10^7	0	0.1	varies

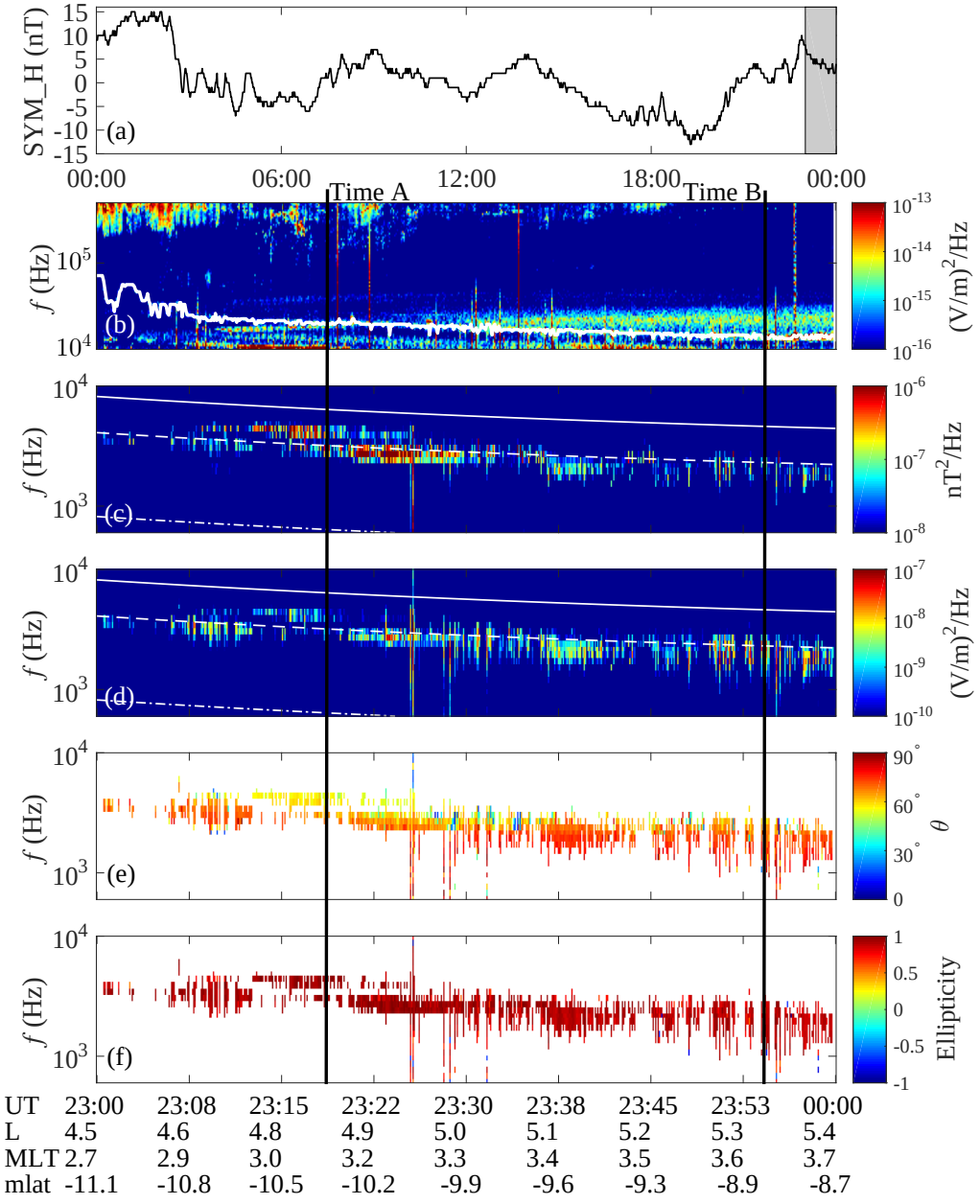

Figure 1. (a) SYM_H index for 3 July 2016. The gray region indicate the period of observation. (b) The electric spectral intensity over 10-500 kHz, (c)the magnetic, and (d) electric spectral intensity, (e) wave normal angle and (f) ellipticity of electromagnetic waves over 0.3-10 kHz observed by Van Allen Probe A during 23-24 UT on 3 July 2016. The white line in Figure 1b marks the upper hybrid resonance frequency (f_{UH}). The white lines in Figures 1c-1d represent $0.1f_{ce}$ (dash dotted), $0.5f_{ce}$ (dashed) and f_{ce} (solid). The vertical lines mark the times when wave local growth rates are calculated on Figure 4.

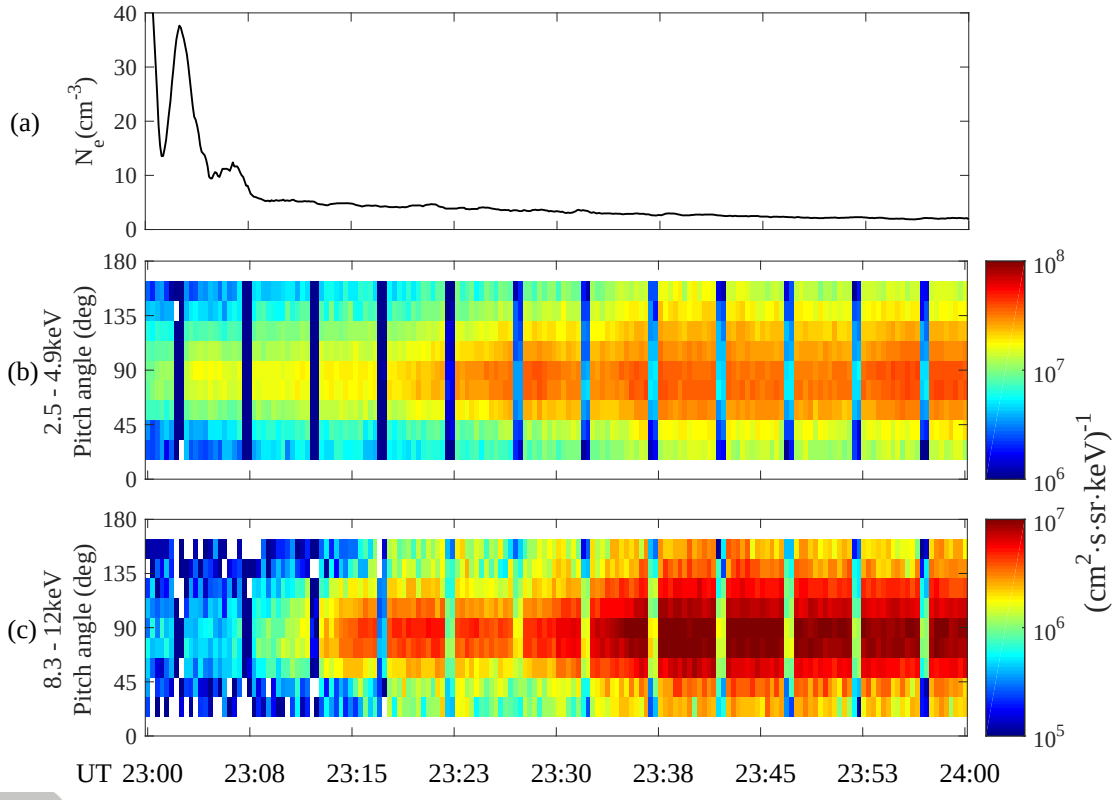

Figure 2. Observations during the interval of oblique chorus waves activity. (a) The measured electron densities derived from the upper hybrid frequency. (b-c) Pitch-angle distributions for 2.5-4.9 keV and 8-12 keV electrons, respectively.

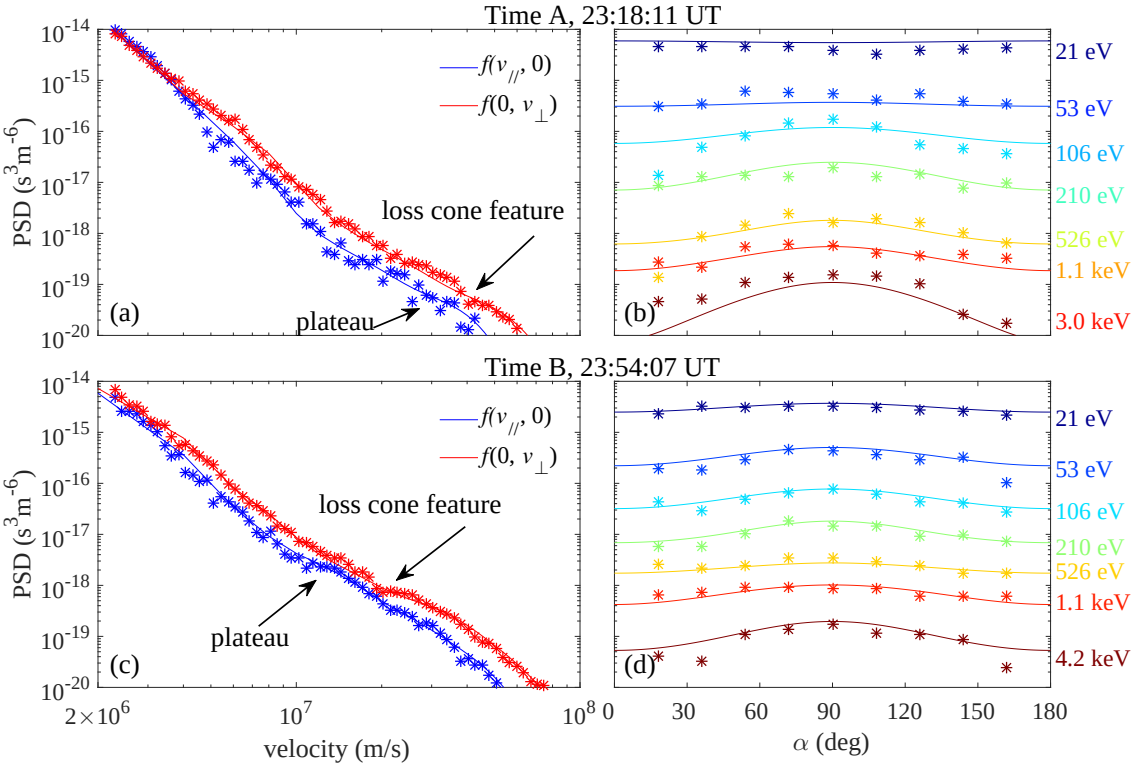

Figure 3. Modeled (solid) and observed (discrete) electron PSD as a function of (a, c) velocity and (b, d) pitch angle. The observed electron PSD was measured by Van Allen Probes at (a-b) times A and (c-d) B, respectively.

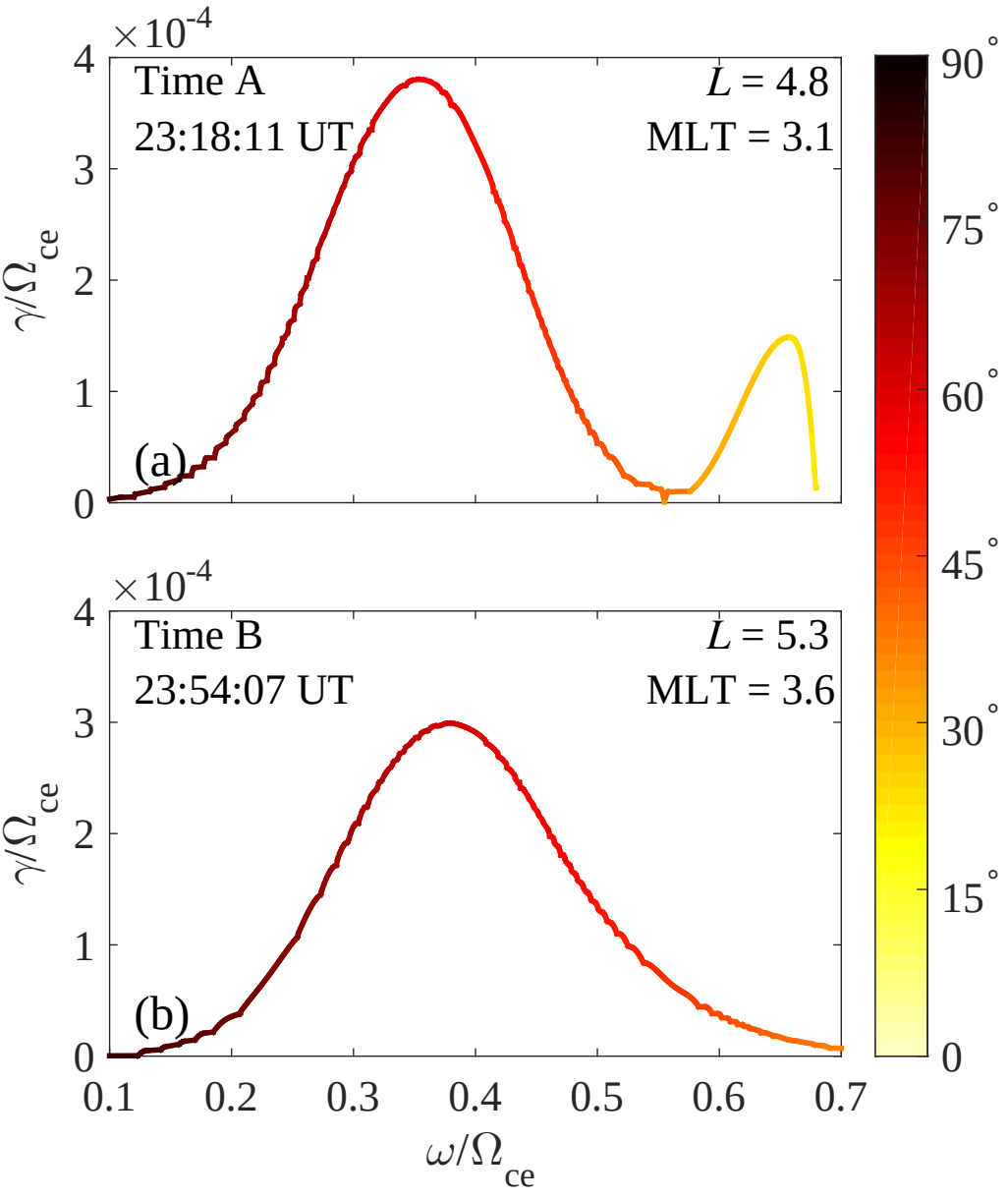

Figure 4. The modeled maximum growth rate corresponding to each wave normal angle θ (color coded) as a function of the wave frequency at times (a) A and (b) B.

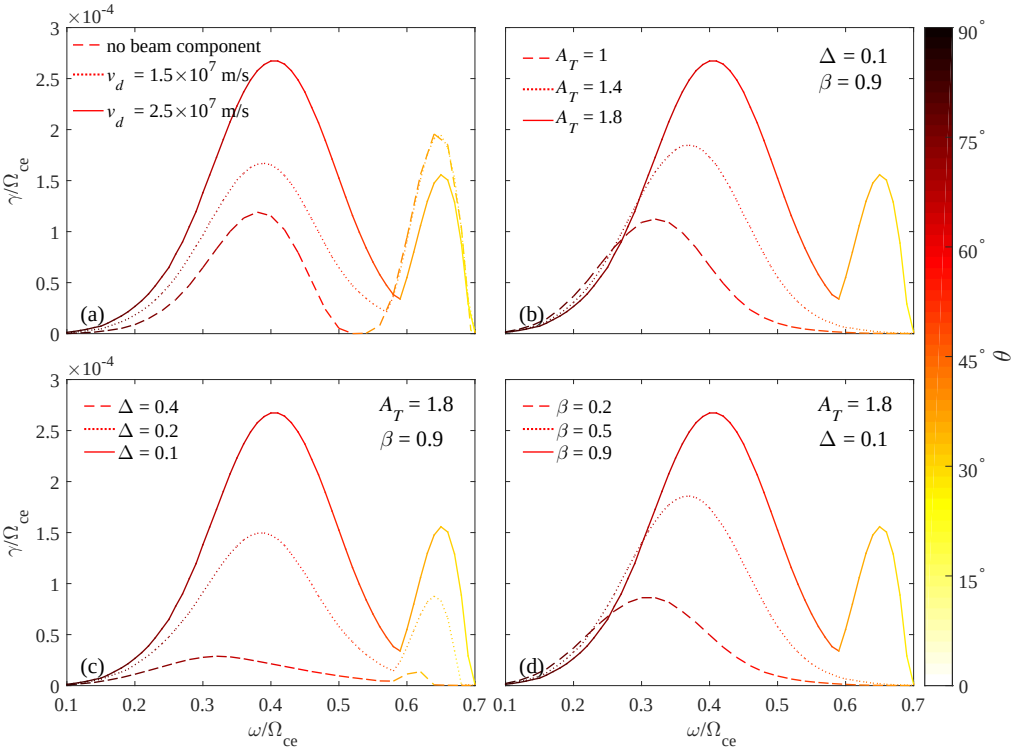

Figure 5. The influence of (a) the beam velocity of the beam component, (b) temperature anisotropy, parameters (c) Δ and (d) β of the subtracted bi-Maxwellian component on the scaled local growth rates. Calculated wave normal angles θ are color coded.